CHEMISTRY OF MATERIALS

ARTICLE

pubs.acs.org/cm

# Phase-Transformation Synthesis of SAPO-34 and a Novel SAPO Molecular Sieve with RHO Framework Type from a SAPO-5 Precursor

Peng Tian,[†] Xiong Su,[†,‡] Yingxia Wang,[§] Qinghua Xia,[∥] Ying Zhang,[†] Dong Fan,[†,‡] Shuanghe Meng,[†] and Zhongmin Liu[†,*]

[†]Dalian National Laboratory for Clean Energy, Dalian Institute of Chemical Physics, Chinese Academy of Sciences, Dalian 116023, P.R. China

[‡]Graduate University of Chinese Academy of Sciences, Beijing 100049, P.R. China

[§]College of Chemistry and Molecular Engineering, Peking University, Beijing 100871, P.R. China

[∥]Ministry-of-Education Key Laboratory for the Synthesis and Application of Organic Functional Molecules, School of Chemistry and Chemical Engineering, Hubei University, Wuhan 430062, P. R. China

Supporting Information

**ABSTRACT:** SAPO-34 and a novel SAPO molecular sieve with the RHO framework (designated as DNL-6) were synthesized using SAPO-5 (the denser phase) as the precursor and diethylamine (DEA) as the template. The entire transition process had been investigated by XRD, SEM, XRF, and NMR spectroscopy, which clearly revealed a solution-mediated transport mechanism attributed to the transformation from SAPO-5 precursor to SAPO-34 via oscillating phases [SAPO-5 (FD = 16.9 T/nm$^3$) => SAPO-34 (15.1) + DNL-6 (14.5) → DNL-6 → SAPO-34]. The initially formed SAPO-34 was different from the final one in this transformation due to very different percentages of organic inclusions, indicating that the host−guest interactions played important roles for the phase selectivity during the synthesis. DNL-6, obtained as an intermediate of the transformation process, possessed good thermal stability, large microporous surface area (724 m$^2$/g), and high micropore volume (0.36 cm$^3$/g). Rietveld refinement showed that the framework of calcined DNL-6 had typical features of the RHO structure with a high symmetry [*I*23, *a* = 15.08429(9) Å], composed of a body-centered cubic arrangement of α cages linked via double 8-rings.

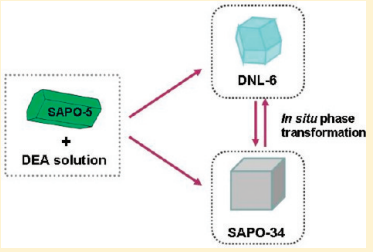


**KEYWORDS:** DNL-6, phase selectivity, phase transformation, RHO, SAPO-34

## 1. INTRODUCTION

Molecular sieves are one of the most important groups of inorganic materials because of their extensive applications in industry as sorbents, ion exchangers, and catalysts.[1,2] At present, more than 190 topologies of molecular sieves with compositional variability have been reported.[3] The progress in materials may create the possibility to establish new industrial processes with high efficiency. Therefore, novel materials and new synthesis methodologies are always the interesting topics in the field of molecular sieves.[4−8]

Molecular sieves are normally synthesized under hydrothermal condition using amorphous gel as the starting material. However, it is sometimes found that the crystallization of one molecular sieve phase is followed by in situ transformation into another phase.[9−13] For example, Dwyer and Chu reported a transition from an amorphous phase to faujasite, and subsequently to ZSM-4 under the help of tetramethylammonium (TMA) cations.[9] Bandyopadhyay et al. found a phase change of an amorphous dry gel → BEA → SSZ-31 → MFI during the synthesis of [Al]-SSZ-31 with a steam-assisted crystallization method.[10] Jhung et al. observed the competition between SAPO-5 and SAPO-34 during the early stage of crystallization where under certain synthesis conditions SAPO-5 disappeared totally and pure SAPO-34 was obtained.[11] Inspired by those in situ phase transformation phenomena, molecular sieves were explored as the synthesis precursors to conduct hydrothermal crystallization, which is an attractive synthesis route and sometimes achieves new products.[14−21] Subotic et al. reported detailed studies of the conversion of A zeolite into sodalite (SOD) and P zeolites (GIS), and concluded that the transition was a solution-mediated process.[14−16] Zones and co-workers also reported serial works on the phase transformation of many zeolites.[17,18] Direct synthesis of Al-SSZ-24 was unsuccessful by a common hydrothermal method and could only be prepared with Al-BEA as the precursor through the phase transition method.[19,20]

Up to now, research on the phase transformation mainly focused on the system of aluminosilicate zeolites, and less emphasis has been put upon SAPO molecular sieves. SAPO-34

**Received:** August 25, 2010
**Revised:** January 17, 2011
**Published:** February 18, 2011

is one of the most important members in the SAPO family, which has been recognized as a good catalyst for the methanol-to-olefin reaction with a high selectivity of ethene and propene.[22,23] During the synthesis of SAPO-34, SAPO-5 is often observed as an intermediate or a competitive phase, implying the possibility of the structure transition between SAPO-5 (AFI topology) and SAPO-34 (CHA topology).[11,12] A SAPO molecular sieve with the RHO structure has not been synthesized to date, though there existed some other RHO zeolite analogues.[24,25] Feng et al. once reported the synthesis of MeAPO-RHO (Me = Co, Mn, and Mg) with *N,N′*-diisopropyl-1,3-propanediamine as the template,[26] but revealed, at the same time, relatively poor thermal stability of thus-prepared MeAPO-RHO with the structure collapse above 753 K.

Herein, we investigate the synthesis of SAPO-34 with SAPO-5 as the precursor. A novel SAPO molecular sieve with the RHO topology has been synthesized. To our best knowledge, it is the first report of the preparation of SAPO molecular sieves via the phase-transformation route. Mechanism studies are carried out in order to understand the transformation process better.

## 2. EXPERIMENTAL SECTION

**2.1. Synthesis.** SAPO-5 was synthesized by a hydrothermal method from the gel with a molar composition of 1.0 triethylamine (TEA): $x$ $SiO_2$:1.0 $Al_2O_3$:0.8 $P_2O_5$:50 $H_2O$ ($x$ = 0.2 or 0.6). The resources for Al, P, and Si were pseudoboehmite (72%), phosphoric acid (85%), and silica sol (25%), respectively. The crystallization was conducted at 448 K for 24 h. SAPO-11 was also explored as the precursor for the phase transformation in the present work, which was crystallized at 473 K for 72 h according to the literature.[27]

A typical procedure for the phase transformation was carried out as follows. Ten grams of as-synthesized SAPO-5 was added to a solution containing 6.5 g of organic amine and 20 g of water under stirring. The resulting mixture was then transferred into an autoclave, which was heated to 473 K within 60 min and kept at this temperature for 16 h under rotation. After the crystallization, the solid product was recovered by filtration, washed with distilled water, and dried in air.

To investigate the phase transformation mechanism, some crystallization experiments were performed in separate batches with different times using the same composition of gels as described above. Once the temperature of autoclave had reached 473 K, the crystallization time was recorded. The mother liquid was collected by centrifuging the quenched reaction mixture at 5000 rmp without addition of water and tightly sealed in glass vials for NMR analysis as soon as possible. The mother liquid had a yellow-brown color with low transparency.

**2.2. Characterization and Structure Solution.** The powder XRD pattern was recorded on a PANalytical X'Pert PRO X-ray diffractometer with Cu Kα radiation ($\lambda$ = 1.54059 Å). The relative weight percentages of SAPO-34 and DNL-6 in the products, calculated from the first peak intensity in the XRD patterns, had been calibrated on the basis of the XRD result of the standard sample (the weight ratio of SAPO-34/DNL-6 = 1) (Figure S1 of the Supporting Information). The chemical composition of the samples was determined with a Philips Magix-601 X-ray fluorescence (XRF) spectrometer. The crystal morphology was observed by scanning electron microscopy (SEM, KYKY-AMRAY-1000B). All NMR experiments were performed on a Varian Infinity plus 400 WB spectrometer with BBO MAS probe operating at a magnetic field strength of 9.4 T. The resonance frequencies were 104.2, 161.9, 79.4, and 100.5 MHz for $^{27}$Al, $^{31}$P, $^{29}$Si, and $^{13}$C, respectively. Chemical shifts were referenced to 1.0 M $Al(NO_3)_3$ for $^{27}$Al, 85% $H_3PO_4$ for $^{31}$P, and 2,2-dimethyl-2-silapentane-5-sulfonate sodium salt (DSS) for $^{29}$Si and $^{13}$C. The spinning rate of the samples at the magic angle was 6 kHz for $^{29}$Si MAS NMR and 8 kHz for $^{13}$C MAS NMR. The pulse delay was 8 s for $^{13}$C MAS NMR. The pH values were measured using a Mettler Toledo acid meter (Seven). $N_2$ adsorption−desorption isotherms were obtained on a Nova 4000 system at 77.35 K. Before analysis, the samples were degassed at 623 K under vacuum. The total surface area was calculated using the BET equation. The microporous volume and surface area were evaluated by the *t*-plot method. The thermal analysis was performed on a TA Q-600 analyzer with a temperature-programmed rate of 10 K/min under an air flow of 100 mL/min.

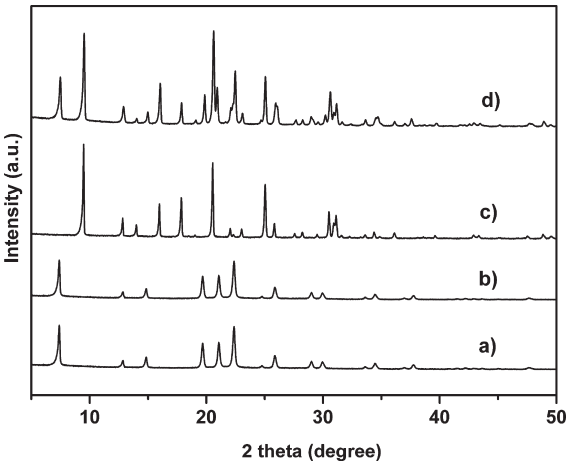


**Figure 1.** XRD patterns of solid products synthesized by the phase transformation method with different templates: (a) the precursor, (b) triethylamine, (c) diethylamine, and (d) morpholine.

Rietveld refinement: Powder X-ray diffraction data were collected at 298 K on a PANalytical X'Pert PRO X-ray diffractometer with Cu Kα radiation ($\lambda$ = 1.54059 Å) in Bragg−Brentano geometry with a plate sample holder and an X'Celerator detector. The scannings were done from 5° to 100° at an increment of 0.0170° with a retention time of 50.17 s per step operating at 40 kV and 40 mA. The comparison of the powder XRD patterns of as-synthesized sample and calcined product indicated that both had the RHO framework and could be indexed by body-centered cubic lattice with the constants of $a$ = 15.1529(1) and 15.08429(9) Å, respectively.[3] Considering the alternative distribution of Al and Si/P atoms in the RHO framework, the space group $I23$ (No. 211) was selected, and the atomic coordinates were deduced from an ideal structure at the Web site of the IZA-structure[3] by the reduction of the space group $Im\text{-}3m$ to $I23$. Rietveld structure refinement of the calcined product was performed by the program Fullprof,[28] in which soft constraints ($d_{Al-O}$ = 1.69 Å and $d_{P/Si-O}$ = 1.60 Å) were applied. The refinement on the whole pattern could lead to either a poor fitting or a divergence. For the zeolite, the low-angle reflection intensities were sensitive to the presence or absence of nonframework species, so that the first two peaks (8.76°, 11.71°) were excluded at the refinement. However, the refinement of the high-angle data (15−100°) was stable and reasonable; therefore, the final refinement was completed in the region of 15−100°.

## 3. RESULTS AND DISCUSSION

**3.1. Synthesis of SAPO-34 by Phase Transformation Method.** Three kinds of organic amines, normally employed as SAPO-34 templates, were tried to explore the possibility of the phase transformation from SAPO-5 to SAPO-34 (Figure 1). Under typical synthesis conditions, diethylamine (DEA) could direct the formation of pure SAPO-34, and morpholine led to the partial transition from SAPO-5 to SAPO-34. However,


dx.doi.org/10.1021/cm103512m |*Chem. Mater.* 2011, 23, 1406–1413

**Table 1. Effect of Diethylamine Amount on Hydrothermal Conversion of SAPO-5 ($T$ = 473K, time = 16 h)**

| | synthesis condition | | | | | | |
|---|---|---|---|---|---|---|---|
| sample | SAPO-5[a] | DEA | $H_2O$ | product[b] | composition | yield | pH[f] |
| 1 | 10 g | 1.5 g | 20 g | SAPO-34 (44.0%) + SAPO-5 (56.0%) | | 80.2% | |
| 2 | 10 g | 2.5 g | 20 g | SAPO-34 (88.7%) + SAPO-5 (11.3%) | | 65.6% | |
| 3 | 10 g | 3.5 g | 20 g | SAPO-34 | $Si_{0.083}Al_{0.499}P_{0.417}$ | 59.5% | |
| 4 | 10 g | 6.5 g | 20 g | SAPO-34 | $Si_{0.092}Al_{0.509}P_{0.399}$ | 52.6% | 11.62 |
| 5 | 10 g | 20.0 g | 20 g | SAPO-34 | $Si_{0.108}Al_{0.497}P_{0.395}$ | 41.2% | 12.38 |
| 6 | 10 g[c] | 4.2 g | 20 g | SAPO-34 | $Si_{0.064}Al_{0.502}P_{0.434}$ | 33.9% | |
| 7 | 10 g[d] | 4.2 g | 20 g | no solid | – | 0 | |
| 8 | 10 g[e] | 4.2 g | 20 g | SAPO-34 | – | 81.7% | |

[a] Elemental composition of SAPO-5: $Si_{0.051}Al_{0.500}P_{0.449}$. [b] The value in the bracket is the relative intensity of the first peak of each phase in the XRD. [c] Elemental composition of SAPO-5: $Si_{0.031}Al_{0.505}P_{0.464}$. [d] The precursor was AlPO-5. [e] The precursor was SAPO-11 ($Si_{0.101}Al_{0.506}P_{0.393}$), $T$ = 473 K, $t$ = 24 h. [f] The pH values of the initial mixtures were 12.23 for sample 4 and 13.03 for sample 5.

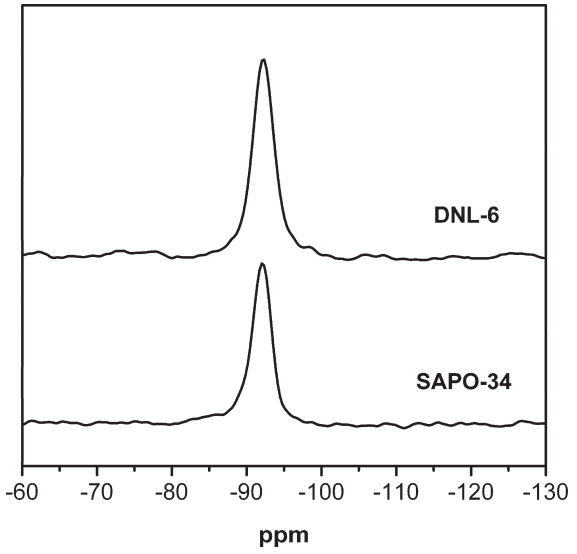


**Figure 2.** $^{29}Si$ MAS NMR spectra of samples synthesized by the phase transformation method.

triethylamine did not initiate any conversion. Therefore, DEA was used as the template for the following researches.

The effect of the DEA amount on the hydrothermal conversion is presented in Table 1. A low amount of DEA could merely convert partial SAPO-5 to SAPO-34. Pure SAPO-34 was obtained with an increased amount of DEA (≥3.5 g), but the product yield decreased inevitably. XRF analysis showed that the Si content in SAPO-34 was higher than that in the SAPO-5 precursor and displayed a rise with the DEA concentration. This could be related to increased alkalinity of the medium, as evidenced by pH values, which increased the solubility of Al, Si, and P species to further promote more Si incorporation into the product, in agreement with our previous findings about the conventional synthesis of SAPO-34 with the DEA template.[29,30] Employing SAPO-5 with lower Si content as the precursor would cause a decrease in the product yield and the Si content in the product (sample 6 in Table 1). No crystal product was formed using AlPO-5 as the precursor. Aside from SAPO-5 with an AFI structure, SAPO-11 with an AEL structure could be successfully transferred into pure SAPO-34 as well (sample 8 in Table 1).

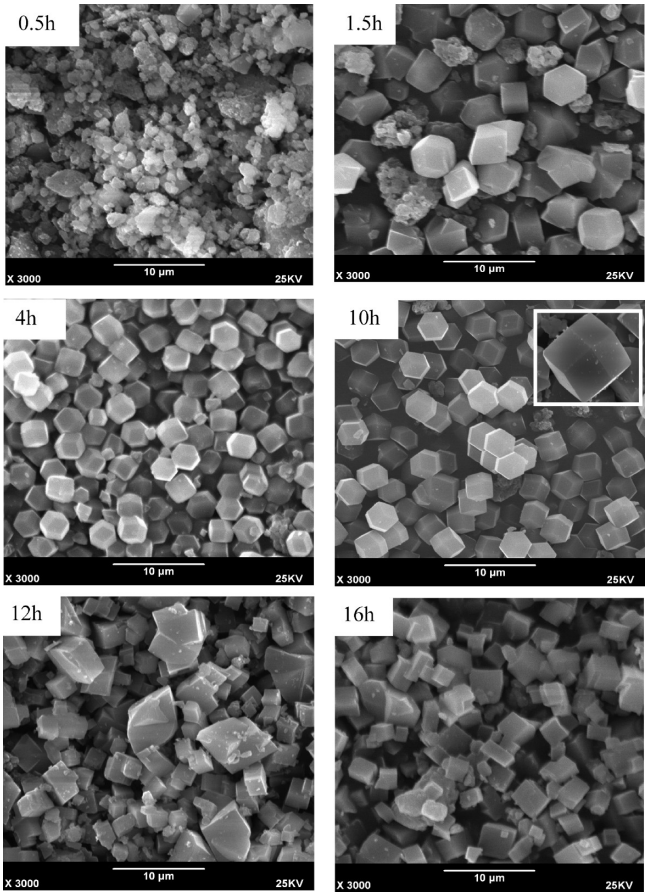


**Figure 3.** SEM images of samples synthesized with different crystallization times. (Crystallization condition: SAPO-5 10 g, DEA 6.5 g, $H_2O$ 20 g, $T$ = 473 K).

$^{29}Si$ MAS NMR spectrum and SEM images of SAPO-34 (sample 4 in Table 1) are shown in Figures 2 and 3. As shown in Figure 3 (16 h), the morphology of crystals is rhombohedral. Only one symmetric peak centered at −92 ppm appeared in the $^{29}Si$ spectrum (Figure 2), ascribable to the $Si(OAl)_4$ species. The textural properties of SAPO-34 obtained from $N_2$ adsorption are shown in Table 2. The microporous surface area and volume were calculated to be 470 $m^2/g$ and 0.24 $cm^3/g$, respectively.


dx.doi.org/10.1021/cm103512m |Chem. Mater. 2011, 23, 1406–1413

Above results indicated the similarity of physical properties of SAPO-34 synthesized by the phase transformation method to those by the common method.[29]

**3.2. Mechanism Investigation of Phase Transformation.** The crystallization with different times using SAPO-5 as the precursor was performed in order to explore the phase transformation mechanism. SEM images and XRD patterns of the solid products are displayed in Figures 3 and 4. The changes of solid and liquid phases following the crystallization time are shown in Table 3. After the crystallization was run at 473K for 0.5 h, only very weak peaks were observed from the XRD pattern of the solid sample, indexed to SAPO-34 (9.4°), gibbsite (18.3°, 18.7°, 20.2° etc.), and pseudoboehmite (broad peaks). A low solid yield (about 1 wt %) at this time indicated that SAPO-5 precursor had been dissolved into the solution. With prolonging the time, the solid yield increased gradually, and the crystal product with a high crystallinity appeared. At $t$ = 1.5 h, the XRD pattern of the solid yield obviously differed from that of any known molecular sieves. Its SEM image revealed that the sample consisted of amorphous phase and two different crystal morphologies of rhombohedra and rhombic dodecahedron, which was therefore inferred to include SAPO-34 and one new material with the RHO structure (named as DNL-6). Along with increasing the crystallization time from 4 to 10 h, pure DNL-6 molecular sieve was achieved. At $t$ > 12 h, DNL-6 disappeared, and SAPO-34 became the only crystal phase.

NMR was employed to investigate the species present in the mother liquid of the initial crystallization mixture (Figure 5). It should be noted that the liquid phase in the present study was not truly homogeneous, and small colloid particles resulting from the normal separation method might coexist.[13] In the $^{27}$Al NMR spectrum of the solution ($t$ = 0.5 h), one strong peak centered at 5 ppm was observed, which can be assigned to octahedral Al species bonded to $HPO_4^{2-}$ ions.[31] The broadness of the peak suggests the low symmetry of Al nuclei and the contribution by many Al-containing species. Moreover, there existed one weak broad peak centered at 60 ppm in the $^{27}$Al NMR spectrum, possibly arising from penta- or tetra-coordinated Al bonded through oxygen to P. This peak became stronger at $t$ = 1.5 h, suggesting that Al species with lower coordination number increased in the liquid phase with the crystallization time. $^{31}$P NMR spectrum at $t$ = 0.5 h contained some sharp resonances (from −5 to 5 ppm), which were contributed by P atoms in

**Table 2. Textual Properties of SAPO-34 and DNL-6 Molecular Sieves**

| | surface area ($m^2$/g) | | | pore volume ($cm^3$/g) | |
|---|---|---|---|---|---|
| sample | $S_{micro}$ | $S_{ext}$ | $S_{total}$ | $V_{micro}$ | $V_{total}$ |
| SAPO-34 [a] | 470 | 53 | 523 | 0.24 | 0.31 |
| DNL-6 [b] | 724 | 0 | 724 | 0.36 | 0.36 |

[a] Sample 4 in Table 1. [b] Sample with the same synthesis condition as sample 4, except crystallization time of 10 h.

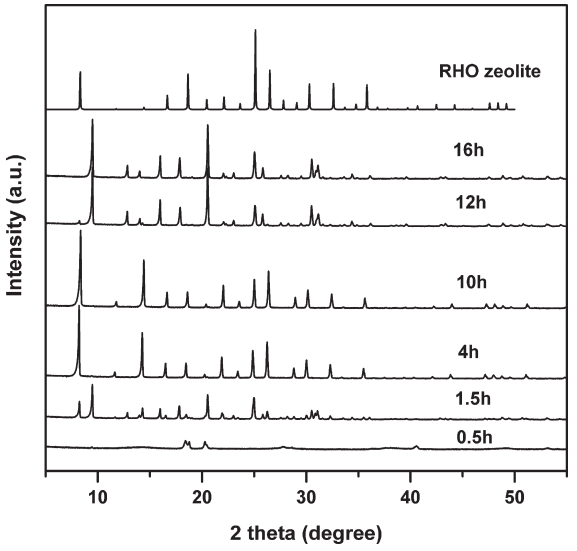


**Figure 4.** XRD patterns of samples synthesized with different crystallization times. The pattern of RHO zeolite is a simulated data. (Crystallizaiton condition: SAPO-5 10 g, DEA 6.5 g, $H_2O$ 20 g, $T$ = 473 K).

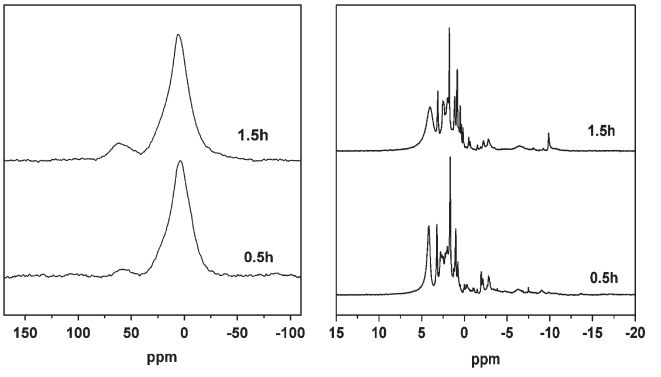


**Figure 5.** $^{27}$Al (left) and $^{31}$P (right) NMR spectra of the mother liquids.

**Table 3. Changes of Solid and Liquid Phases during Hydrothermal Conversion[a]**

| | | | inorganic composition | | |
|---|---|---|---|---|---|
| time | product[b] | yield | solid phase | liquid phase[c] | pH |
| 0.5 h | SAPO-34 (tiny) + gibbsite pseudoboehmite | 1.0% | − | $Si_{0.051}Al_{0.472}P_{0.478}$ | 11.13 |
| 1.5 h [d] | SAPO-34 (76.3%) + DNL-6 (23.7%) | 7.0% | $Si_{0.083}Al_{0.592}P_{0.325}$ | $Si_{0.045}Al_{0.473}P_{0.482}$ | 11.10 |
| 4 h | DNL-6 (99.2%) + SAPO-34 (0.8%) | 29.0% | $Si_{0.136}Al_{0.502}P_{0.372}$ | − | 11.32 |
| 10 h | DNL-6 | 37.6% | $Si_{0.130}Al_{0.506}P_{0.364}$ | $Si_{0.006}Al_{0.511}P_{0.483}$ | 11.45 |
| 12 h | SAPO-34 (97.0%) + DNL-6 (3.0%) | 47.8% | $Si_{0.092}Al_{0.504}P_{0.404}$ | $Si_{0.008}Al_{0.469}P_{0.523}$ | 11.56 |
| 16 h | SAPO-34 | 52.6% | $Si_{0.092}Al_{0.509}P_{0.399}$ | − | 11.62 |

[a] SAPO-5 10 g, DEA 6.5 g, $H_2O$ 20 g, $T$ = 473 K. [b] The value in the bracket was the relative weight content of each phase in the crystalline products. [c] The solution was first evaporated at 353K, and then analyzed by XRF. [d] The sample contained ~30 wt % of amorphous solid.


dx.doi.org/10.1021/cm103512m |Chem. Mater. 2011, 23, 1406–1413

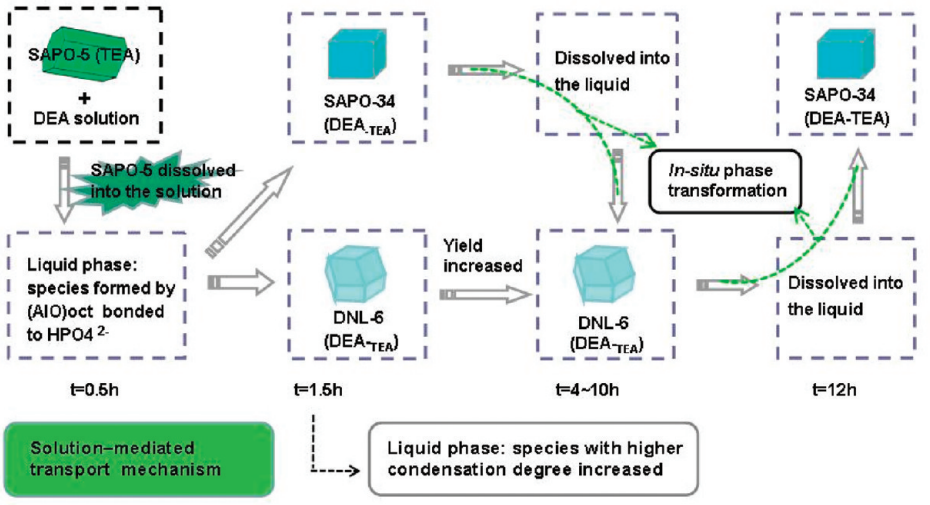


**Figure 6.** Schematic overview of the proposed phase transformation mechanism.

aluminophosphate complexes, i.e., $HPO_4^{2-}$ ions bonded to Al species. After 1.5 h, one more peak at −10 ppm appeared in the $^{31}$P NMR spectrum. According to the literature,[31−33] the chemical shift of the P atom becomes more negative with an increase in its partial charge. Therefore, it can be speculated that the appearance of new peak could result from P species in aluminophosphate complexes with a higher condensation degree, which would cause an increase in the partial charge of P nuclei.

On the basis of the above results, the phase transformation mechanism is schematically illustrated in Figure 6. Supposedly, SAPO-5 was first dissolved into the solution to destroy basic building units and to form soluble octahedral Al species and $HPO_4^{2-}$ ions during crystallization. Then, those species with a higher condensation degree appeared in the solution, together with the formation of crystal products. SAPO-34 and DNL-6 were crystallized through the solution-mediated transport mechanism.

**3.3. Investigation of in situ Phase Transformation.** An interesting phenomenon during the hydrothermal conversion is that there existed twice in situ phase transformations, i.e., AFI (FD = 16.9 T/nm$^3$) => CHA (FD = 15.1) → RHO (FD = 14.5) → CHA.[3] These transitions could be relevant to the phase selectivity, which is a fundamental question, but still not well understood presently.[34−36]

The pH values of mother liquids with different times showed that the phase transformation occurred under strong basic conditions (Table 3). At the early crystallization stage of $t \leq$ 1.5 h, the pH value of mother liquid was lowered down to about 11.10, as compared with the initial value of 12.23. This could be due to the consumption of DEA used for the dissolution of SAPO-5. At the end of the hydrothermal conversion, the pH value displayed a slight increase to 11.62. XRF analysis indicated gradual changes of the elemental compositions of solids and liquids during the crystallization process. The the Si content in the final SAPO-34 was lower than that in DNL-6, but both were higher than that in the precursor, which could be the main reason responsible for low solid yields.

$^{13}$C MAS NMR spectra of as-synthesized samples are presented in Figure 7. The small signal at 32 ppm was a ghostpeak, which would disappear in the corresponding $^1$H → $^{13}$C CP MAS NMR spectra or with changing the spinning speeds (Figures S2 and S3 of the Supporting Information). No signal was observed from the spectrum at $t$ = 0.5 h, indicating the absence of organic amine in the solid. Afterward, the signals from both DEA and TEA appeared in the spectra, suggesting the coexistence of two amines (TEA was released from the SAPO-5 precursor). The deconvoluted results revealed that the molar ratios of DEA/TEA in the samples changed always with time (Figure 7). In the sample with $t$ = 1.5 h, the DEA content was higher than TEA (DEA/TEA = 5.26). After 4 h, DNL-6 appeared as one major phase, but the molar ratio of DEA/TEA decreased from 9.09 to 5.88 ($t$ = 10 h). Subsequently, the molar ratio of DEA/TEA showed a sharp drop to 1.18 at $t$ = 16 h, accompanied with the

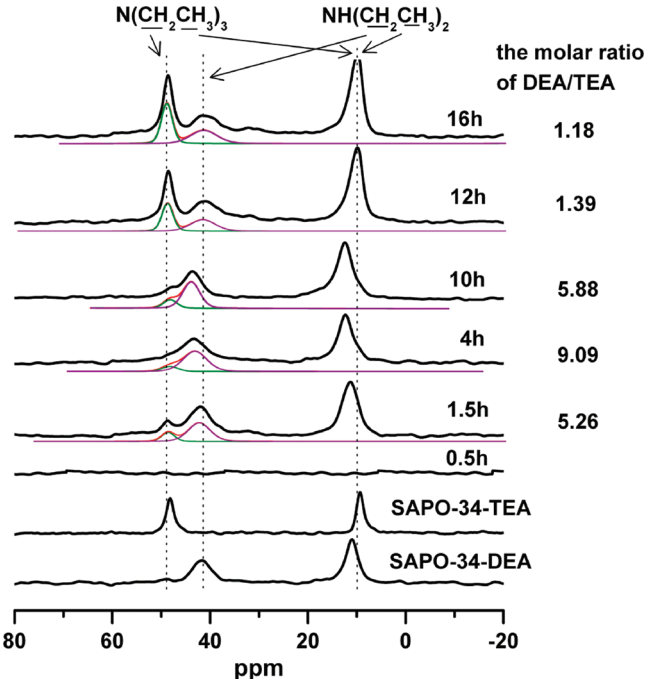


**Figure 7.** $^{13}$C MAS NMR spectra of samples with different crystallization times. SAPO-34-TEA and SAPO-34-DEA were synthesized with TEA and DEA templates, respectively. They were used as standard samples.


dx.doi.org/10.1021/cm103512m |Chem. Mater. 2011, 23, 1406–1413

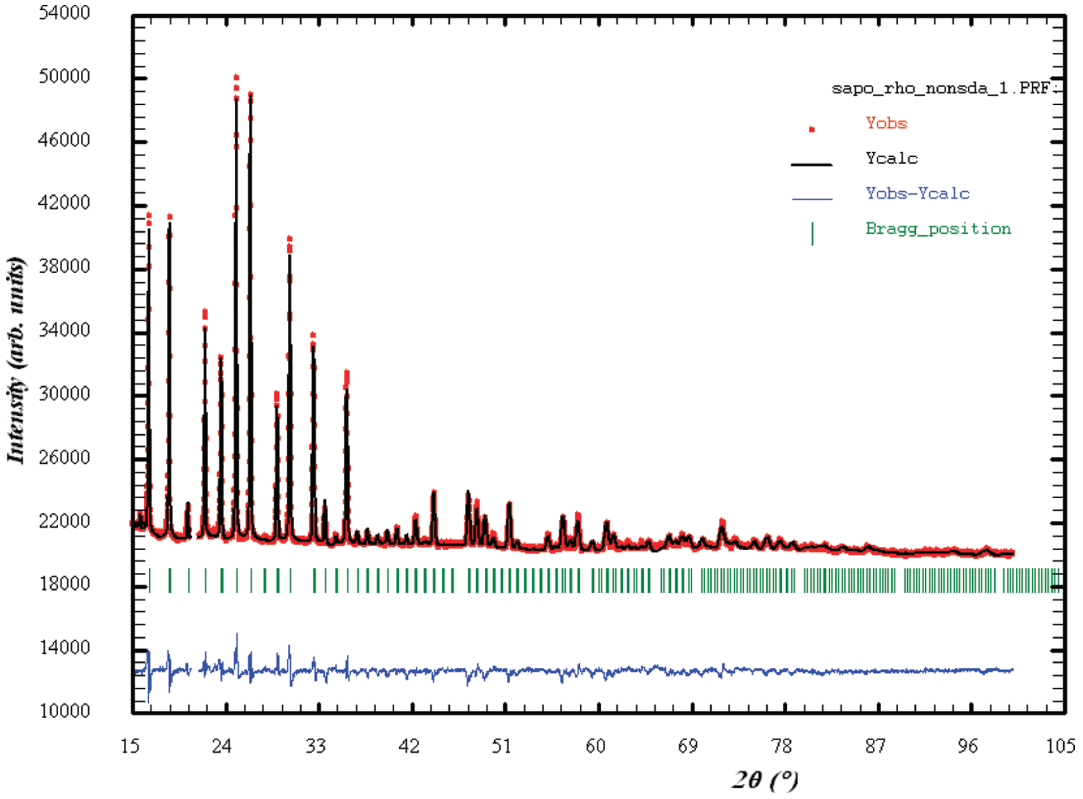


**Figure 8.** Rietveld analysis plot of the powder X-ray diffraction pattern of calcined DNL-6. The dot symbol represents the observed pattern, and the solid line is the calculated pattern. The bars below the diffraction curves are the Bragg reflection positions, and the difference curve is shown at the bottom.

formation of pure SAPO-34. The molar ratio of DEA/TEA in the initially formed SAPO-34 (at 1.5 h) was roughly estimated to be 4.40, by assuming that the DEA/TEA ratio in DNL-6 was kept unchanged from 1.5 to 4 h (Part S1 of the Supporting Information). Clearly, TEA had joined the whole crystallization process to exert an important impact on the formation of the final SAPO-34, though its concentration in the solution was relatively small (DEA/TEA ratio ≈11).

Thus, it can be inferred that the in situ phase transformation could work very well according to a liquid-phase mechanism, similar to the initial transformation of SAPO-5 precursor. The percentage of organic inclusions in the products varied with the crystallization process. Generally, the phase transition process could follow the sequence of SAPO-34 (DEA-$_{TEA}$) → DNL-6 (DEA-$_{TEA}$) → SAPO-34 (DEA-TEA), meaning that the stability was SAPO-34 (DEA-$_{TEA}$) < DNL-6 (DEA-$_{TEA}$) < SAPO-34 (DEA-TEA). These results revealed that the host−guest interactions played important roles in the crystallization of molecular sieves, and the phase selectivity was not only determined by the framework stability. Recently, Zicovich-Wilson et al. studied the in situ transformation from TON topology to less dense ITW by periodic ab initio calculations for the first time and concluded that the structure direction, by virtue of host−guest interactions in the as-made materials, could overcome the thermodynamic penalty of producing a less stable framework.[37] This is consistent with our present results.

**3.4. Characterization and Structure Solution of DNL-6 Molecular Sieve.** From the SEM image of the sample (10 h) in Figure 3, only crystals with the morphology of rhombic dodecahedron can be found, indicating the high purity of DNL-6 synthesized in the present study. The elemental analysis of DNL-6 by XRF gave a molar composition of $Si_{0.130}Al_{0.506}P_{0.364}O_2$, suggesting that all Si atoms in DNL-6 existed as Si(4Al) coordination in the framework (SM2 mechanism), which was further verified by only one symmetric peak centered at −92 ppm in the $^{29}$Si MAS NMR spectrum (Figure 2). The framework

**Table 4. Crystallographic Data and Results of Rietveld Analysis of DNL-6**

| | |
|---|---|
| formula | $H_{3.12}[Al_{12}Si_{3.12}P_{8.88}O_{48}]$ |
| crystal system | cubic |
| space group | *I*23 |
| *a* (Å) | 15.08429(9) |
| *Z* | 2 |
| λ (Å) | 1.5406 |
| range 2θ (deg) | 5.0 −99.983 |
| excluded regions | 5−15 |
| step width 2θ (deg) | 0.0170 |
| number of points | 5582 |
| number of restraints | 8 |
| number of fitted parameters | 27 |
| peak profile | Thompson−Cox−Hastings pseudo-Voigt |
| background correction | linear interpolation of background points |
| *R*wp | 0.116 |
| *R*exp | 0.0865 |
| $\chi^2$ | 1.81 |


dx.doi.org/10.1021/cm103512m |*Chem. Mater.* 2011, 23, 1406–1413

**Table 5. Atomic Coordinates, Isotropic Thermal Displacement Parameters, and Bond Valence Sum (BVS) for DNL-6**

| atom | Wyckoff site | *x* | *y* | *z* | *B* (Å$^2$) | Occu | BVS |
|---|---|---|---|---|---|---|---|
| Al | 24*j* | 0.2586(2) | 0.4037(2) | 0.1031(2) | 1.45 | 1.00 | 3.29 |
| Si | 24*j* | 0.2482(2) | 0.8877(2) | 0.6023(2) | 1.45 | 0.26 | 4.43 |
| P | 24*j* | 0.2482(2) | 0.8877(2) | 0.6023(2) | 1.45 | 0.74 | 4.43 |
| O1 | 24*j* | 0.2138(3) | 0.0120(2) | 0.3891(4) | 1.99 | 1.00 | 1.91 |
| O2 | 24*j* | 0.0000(2) | 0.2237(4) | 0.6220(4) | 1.99 | 1.00 | 1.89 |
| O3 | 24*j* | 0.1601(2) | 0.1678(3) | 0.3762(3) | 1.99 | 1.00 | 1.95 |
| O4 | 24*j* | 0.1742(3) | 0.1777(2) | 0.6365(3) | 1.99 | 1.00 | 1.96 |

**Table 6. Selected Distances and Angles for DNL-6**

| atom−atom | bond length (Å) | atom−atom−atom | bond angle (deg) |
|---|---|---|---|
| Al−O1 | 1.699(4) | O1−Al−O2 | 111.3(5) |
| Al−O2 | 1.703(9) | O1−Al−O3 | 114.0(4) |
| Al−O3 | 1.685(5) | O1−Al−O4 | 122.7(3) |
| Al−O4 | 1.685(5) | O2−Al−O3 | 99.3(5) |
| Si/P−O1 | 1.587(4) | O2−Al−O4 | 107.4(5) |
| Si/P−O2 | 1.591(9) | O3−Al−O4 | 99.2(4) |
| Si/P−O3 | 1.584(5) | O1−Si/P-O2 | 104.4(5) |
| Si/P−O4 | 1.581(5) | O1−Si/P-O3 | 102.0(4) |
| | | O1−Si/P-O4 | 112.7(4) |
| | | O2−Si/P-O3 | 111.4(5) |
| | | O2−Si/P-O4 | 116.5(5) |
| | | O3−Si/P-O4 | 108.8(4) |

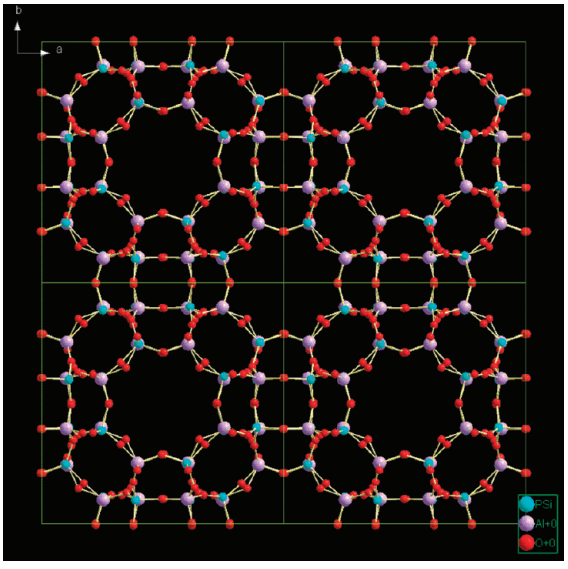

**Figure 9.** Stereoview of the framework structure of DNL-6 obtained from the structure refinement, viewed down the *c* axis. (Al atoms in purple, P/Si atoms in blue, and O atoms in red).

of DNL-6 composed of high concentration of Si(4Al) environment could be ascribed to the easy inclusion of the DEA template with small size into large LTA cage in the RHO structure.[38]

After being calcined in air at 873 K for 3 h, DNL-6 was homogeneously microporous and gave a typical Type I adsorption isotherm (Figure S4 of the Supporting Information). The microporous surface area and volume were determined to be 724 m$^2$/g and 0.36 cm$^3$/g, respectively. Moreover, the thermal analysis of DNL-6 showed that a high weight loss of ∼22 wt % was due to the removal of water and template occluded in the cages of RHO structure, well in agreement with its large pore volume (Figure S5 of the Supporting Information).

On the basis of the framework topology of the RHO zeolite, the Rietveld refinement of calcined DNL-6 (indexed into the space group *I*23) was performed by Fullprof with refined unit cell parameter $a$ = 15.08437(9) Å. The value was close to that of H-type RHO without framework distortion (a ≈ 15.1 Å). Figure 8 displays the plots of the Rietveld refinement result. Tables 4, 5, and 6 list the crystallographic data of DNL-6, atomic coordinates, and bond valence sums as well as the selected bond lengths and angles for Rietveld analysis, respectively. The values and ranges for T−O lengths and O−T−O angles were set in a reasonable range for SAPO/AlPO structures. The bond valence sums also confirmed the proper locations of $Al^{3+}$ and $P^{5+}/Si^{4+}$ in the framework. Figure 9 shows the skeletal model of the refined framework structure. Clearly, the framework of DNL-6 exhibits typical features of the RHO structure with a high symmetry, composed of a body-centered cubic arrangement of α cages linked via double 8-rings.[3]

## 4. CONCLUSIONS

Pure SAPO-34 and a novel SAPO molecular sieve with the RHO topology (named as DNL-6) were synthesized using SAPO-5 as the precursor and DEA as the template. The phase transformation occurred according to a liquid-phase transport mechanism, in which SAPO-5 was first dissolved into the solution to destroy its building units completely. SAPO-34 (DEA-$_{TEA}$) and DNL-6 (DEA-$_{TEA}$) were crystallized as the intermediates. Subsequently, the former was dissolved to yield pure DNL-6, which could stably exist for several hours until it was totally converted to pure SAPO-34 (DEA-TEA). The percentage of organic inclusions in the products varied throughout the crystallization process. The phenomena of in situ oscillating phase transformations revealed that the phase stability was related to not only the topology but also to the mutual interactions between the framework and the inclusions in the pores and cavities. The novel small-pore molecular sieve DNL-6 possessed good thermal stability, high surface area, and large pore volume. The framework of DNL-6 composed of high concentration of Si(4Al) environment could be ascribed to the easy inclusion of the DEA template with small size into large LTA cage in the RHO structure. The formation of DNL-6 implied that the phase transformation method could be a potential route for exploring the synthesis of new types of molecular sieves.

## ■ ASSOCIATED CONTENT

**Ⓢ Supporting Information.** XRD pattern, $^{13}$C MAS NMR spectra, $^{1}$H → $^{13}$C CP MAS NMR spectra, thermal analyses, $N_2$ adsorption isotherms, and the calculation method for the molar ratio of DEA/TEA. This material is available free of charge via the Internet at http://pubs.acs.org.

## ■ AUTHOR INFORMATION

**Corresponding Author**

*E-mail: liuzm@dicp.ac.cn. Tel: 0086-411-84379149. Fax: 0086-411-84379289.

## ■ ACKNOWLEDGMENT

We gratefully thank Dr. Shutao Xu for his assistance in the NMR experiments.

## ■ REFERENCES

(1) Wright, P. A. *Microporous Framework Solids*; RSC Publishing: Cambridge, U.K., 2007.
(2) Davis, M. E. *Nature* **2002**, *417*, 813.
(3) Database of Zeolite Structures. http://www.iza-structure.org/databases/.
(4) Hari Prasad Rao, P. R.; Matsukata, M. *Chem. Commun.* **1996**, 1441.
(5) Cooper, E. R.; Andrews, C. D.; Wheatley, P. S.; Webb, P. B.; Wormald, P.; Morris, R. E. *Nature* **2004**, *430*, 1012.
(6) Boix, T.; Puche, M.; Camblor, M. A.; Corma, A. U.S. Patent 6,471,941, 2002.
(7) Burton, A.; Elomari, S.; Chen, C. Y.; Medrud, R. C.; Chan, I. Y.; Bull, L. M.; Kibby, C.; Harris, T. V.; Zones, S. I.; Vittiratos, E. S. *Chem.—Eur. J.* **2003**, *9*, 5737.
(8) Pastore, H. O.; de Oliveira, E. C.; Superti, G. B.; Gattiand, G.; Marchese, L. *J. Phys. Chem. C* **2007**, *111*, 3116.
(9) Dwyer, F. G.; Chu, P. *J. Catal.* **1979**, *59*, 263.
(10) Bandyopadhyay, R.; Kubota, Y.; Ogawa, M.; Sugimoto, Y. F.; Sugi, Y. *Chem. Lett.* **2000**, *29*, 300.
(11) Jhung, S. H.; Chang, J. S.; Hwang, J. S.; Park, S. E. *Microporous Mesoporous Mater.* **2003**, *64*, 33.
(12) Venna, S. R.; Carren, M. A. *J. Mater. Chem.* **2009**, *19*, 3138.
(13) Cundy, C. S.; Cox, P. A. *Microporous Mesoporous Mater.* **2005**, *82*, 1.
(14) Subotic, B.; Skrtic, D.; Smit, I.; Sekovanic, L. *J. Cryst. Growth* **1980**, *50*, 498.
(15) Subotic, B.; Sekovanic, L. *J. Cryst. Growth* **1986**, *75*, 561.
(16) Subotic, B.; Smit, I.; Madzija, O.; Sekovanic, L. *Zeolite* **1982**, *2*, 135.
(17) Zones, S. I. *J. Chem. Soc., Faraday Trans.* **1991**, *87*, 3709.
(18) Zones, S. I.; Nakagawa, Y. . *Microporous Mesoporous Mater.* **1994**, *2*, 557.
(19) Maekawa, H.; Kubota, Y.; Sugi, Y. *Chem. Lett.* **2004**, *33*, 1126.
(20) Kubota, Y.; Maekawa, H.; Miyata, S.; Tatsumi, T.; Sugi, Y. *Microporous Mesoporous Mater.* **2007**, *101*, 115.
(21) Inoue, T.; Itakura, M.; Jon, H.; Oumi, Y.; Takahashi, A.; Fujitani, T.; Sano, T. *Microporous Mesoporous Mater.* **2009**, *122*, 149.
(22) Liu, Z. M.; Sun, C. L.; Wang, G. W.; Wang, Q. X.; Cai., G. Y. *Fuel Process. Technol.* **2000**, *62*, 161.
(23) Wilson, S. T.; Barger, P. T. *Microporous Mesoporous Mater.* **1999**, *29*, 117.
(24) Robson, H. E. U.S. Patent 3,720,753, 1973.
(25) Newsam, J. M.; Vaughan, D. E. W.; Strohmaier, K. G. *J. Phys. Chem.* **1995**, *99*, 9924.
(26) Feng, P. Y.; Bu, X. H.; Stucky, G. D. *Microporous Mesoporous Mater.* **1998**, *23*, 315.
(27) Lok, B. M.; Messina, C. A.; Patton, R. L.,; Gajek, R. T.; Cannan, T. R.; Flanigen, E. M. U.S. Patent 4,440,871, April 3, 1984.
(28) Rodriguez-Carvajal, J. *Phys. B.* **1993**, *192*, 55–69.
(29) Liu, G. Y.; Tian, P.; Li, J. Z.; Zhang, D. Z.; Zhou, F.; Liu., Z. M. *Microporous Mesoporous Mater.* **2008**, *111*, 143.
(30) Liu, G. Y.; Tian, P.; Zhang, Y.; Li, J. Z.; Xu, L.; Meng, S. H.; Liu., Z. M. *Microporous Mesoporous Mater.* **2008**, *114*, 4163.
(31) Mortlock, R. F.; Bell, A. T.; Radke, C. J. *J. Phys. Chem.* **1993**, *97*, 767.
(32) Mortlock, R. F.; Bell, A. T.; Radke, C. J. *J. Phys. Chem.* **1993**, *97*, 775.
(33) Vistad, Ø. B.; Hansen, W. W.; Akporiaye, D. E.; Lillerud, K. P. *J. Phys. Chem. A* **1999**, *103*, 2540.
(34) Burton, A. W.; Zones, S. I.; Elomari, S. *Curr. Opin. Colloid Interface Sci.* **2005**, *10*, 211.
(35) Burton, A. W.; Lee, G. S.; Zones, S. I. *Microporous Mesoporous Mater.* **2006**, *90*, 129.
(36) Piccione, P. M.; Yang, S.; Navrotsky, A.; Davis, M. E. *J. Phys. Chem. B* **2002**, *106*, 3629.
(37) Zicovich-Wilson, C. M.; Gandara, F.; Monge, A.; Camblor, M. A. *J. Am. Chem. Soc.* **2010**, *132*, 3461.
(38) Bu, X. H.; Feng, P. Y.; Stucky, G. D. *Science* **1997**, *278*, 2080.